2023 62nd IEEE Conference on Decision and Control (CDC)
December 13-15, 2023. Marina Bay Sands, Singapore

Fourth-order reference trajectories in lithography stages with weakly-damped modes – a frequency-domain perspective

Marcel Heertjes[1], Jazmin Zenteno Torres[2], and Mohammad Al Janaideh[3]

***Abstract*— The tracking accuracy in motion control systems like the moving stages in lithography machines, *e.g.,* wafer scanners or metrology inspection tools, is partly determined by how the frequency content of its reference trajectories is transferred to the closed-loop tracking error. In this regard, fourth-order reference trajectories for point-to-point motion will be studied from a frequency-domain perspective. By appropriately pairing the maximum snap and maximum jerk values, weakly-damped modes in the closed-loop response can be robustly dealt with without introducing a penalty on throughput.**

I. Introduction

In the semiconductor industry, stage systems, like the reticle and wafer stages in wafer scanners, perform nano-positioning tasks under aggressive tracking motions [1]. To meet the ever-tightening specifications in stage error budgets, stage design relies on control. First, feedback control of the multivariable stage system in the presence of disturbances like shown in Butler [2]. Second, feedforward control to deal with tracking of the rigid- as well as the non-rigid body stage dynamics; illustrative is the initial work on snap feedforward control by Boerlage et al. [3], with data-based parameter tuning by Van der Meulen et al. [4], brought into the instrumental variables framework by Boeren et al. [5], and often replaced by linear parameter varying methods as described in Kontaras et al. [6]. Third, design and shaping of its reference trajectories, which is the topic of this paper.

Input shaping has a long history in motion control systems. Dating back to 1957, posicast control [7], [8] by Smith reflected the idea of convolving a 2-pulse sequence with a step input as a means for a dynamic system to move forward without vibration. The idea was further developed by Seering and co-workers [9] in the 1980's who considered general finite impulse response filters, essentially notch filters, for the convolution, and introduced robustness to modelling error during the late 1980's and early 1990's by the zero vibration and derivative (ZVD) shaper and the extra-insensitive (EI) shaper, as in Singhose, Seering & Singer [10] and the references therein, but also the work of Pao [11], as well as the overview by Singhose [12] that covers a broader historical perspective. Recent analysis using impulse vectors can be found in the work of Kang et al. [13].

Though proven effective as a technique for motion control by numerous applications, input shapers do come with a penalty on the move time [14]. For point-to-point motions in wafer scanners, this translates directly into a penalty on throughput. Shaping the input in wafer scanners is therefore done by exploiting the freedom in designing the snap-over-jerk and jerk-over-acceleration ratios instead, which still comes close to the original idea of posicast control. Namely, the jerk step input is convolved with a snap pulse sequence, which connects to the work of Béarée [15] on damped-jerk trajectory analysis. By adjusting the width and height of the jerk and snap steps, the spectrum of the input can be designed to have no spectral content at specific frequencies without introducing a penalty on throughput. By matching these frequencies (zeros) or multiples thereof with the frequencies (poles) of weakly-damped modes of the stage system that hamper tracking performance, vibrations in the tracking error response can be mitigated. In this regard, the work of Al-Rawashdeh at al. [16] on second- and third-order trajectories is of interest. For higher-order motions, Sencer & Tajima [17], Sencer et al. [18], and Dumanli & Sencer [19] show attenuation of spectral energy in desired frequency bands.

This paper has two contributions. First, a formal frequency-domain analysis is given of fourth-order reference trajectories; see also Van den Biggelaar et al. [20] and Lambrechts et al. [21] for a time-domain design, the early work by Singh & Vadali [22] for robust time-optimal control using a frequency-domain approach, and the work of Bai et al. [23] on time-optimal third-order trajectories. The main result will be a parametric representation of the spectral content that can be used for trajectory generation and design. Second, a design criterion is presented for finding the maximum jerk and snap values (under fixed maximum values of acceleration and velocity) that minimize the closed-loop error signals in the $\mathcal{L}_\infty$ sense (and in the presence of weakly-damped stage modes) in a throughput-invariant manner; the works of Miu & Bhat [24] and Al-Masoud et al. [25] consider minimizing the $\mathcal{L}_2$ norm, but without constraining the order.

The remainder of the paper is organized as follows. In Section II, the motion control context is given and the stage tracking problem is formulated. In Section III, a frequency-domain analysis of fourth-order reference trajectories is presented, whereas in Section IV the design criterion is presented as well as the results obtained from a simplified stage model. In Section V, the main conclusions are summarized.

[1]Marcel Heertjes is with Department of Mechanical Engineering, Control Systems Technology group, Eindhoven University of Technology, The Netherlands m.f.heertjes@tue.nl and also with ASML, D&E wafer stage control group, The Netherlands

[2]Jazmin Zenteno Torres is with ASML, Research mechatronics group, The Netherlands jazmin.zentenotorres@asml.com

[3]Mohammad Al Janaideh is with the Department of Mechanical Engineering, Memorial University, St. John's Newfoundland, and with the School of Engineering, University of Guelph, Guelph, ON N1G 2W1, Canada. maljanaideh@mun.ca.

II. Tracking problem formulation

Consider the motion control setting in Fig.1 with stage

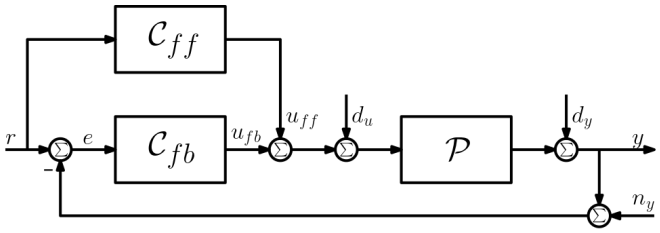

Fig. 1. Motion control setting.

system $\mathcal{P}$, feedback controller $\mathcal{C}_{fb}$, feedforward controller $\mathcal{C}_{ff}$, all being represented (for the sake of simplicity) by single-input single-output (SISO) systems. Furthermore, let reference r, input/output disturbances d_u, d_y, and sensor noise n_y be the inputs, and the stage position y the single output. The stage system $\mathcal{P}$ can be modelled as

$$\mathcal{P}(\omega) = \underbrace{-\frac{1}{m\omega^2}}_{\mathcal{P}_{rb}(\omega)} + \underbrace{\sum_{i=1}^{\infty} \frac{c_i}{\omega^2 - 2\zeta_i\omega_i j\omega - \omega_i^2}}_{\mathcal{P}_{nrb}(\omega)}, \tag{1}$$

with m the mass of the rigid body mode and ζ_i, ω_i, c_i the dimensionless damping, natural frequency, and scaling factor, respectively, of the i-th non-rigid body mode. In achieving appropriate tracking performance, i.e., $y(\omega) \to r(\omega)$, the nominal feedforward controller is generally designed as

$$\mathcal{C}_{ff}(\omega) = \mathcal{P}_{rb}^{-1}(\omega) = -m\omega^2. \tag{2}$$

By assuming all the inputs to be the result of zero-mean white-noise processes except for the reference signal r, the transfer from reference trajectory r to tracking error $e = r - y$ with feedforward controller (2), and by neglecting the remaining inputs, is given by

$$\begin{aligned} e(\omega) &= \frac{(1 - \mathcal{C}_{ff}(\omega)\mathcal{P}(\omega))}{1 + \mathcal{C}_{fb}(\omega)\mathcal{P}(\omega)} \cdot r(\omega) \\ &= -\frac{\mathcal{P}_{rb}^{-1}(\omega)\mathcal{P}_{nrb}(\omega)}{1 + \mathcal{C}_{fb}(\omega)\mathcal{P}(\omega)} \cdot r(\omega). \end{aligned} \tag{3}$$

Remark 2.1: Wafer scanning is done under constant velocity during exposure [1]. As such, the tracking error e in (3) should be minimized in the $\mathcal{L}_2$ or $\mathcal{L}_\infty$-sense within the exposure interval, for example by minimizing $\|e\|_2$ or $\|e\|_\infty$.

Example 2.1: Consider a fourth-order stage model

$$\begin{aligned} \mathcal{P}(\omega) &:= -\frac{1}{m\omega^2} + \frac{c_1(\omega)}{\omega^2 - 2\zeta_1\omega_1 j\omega - w_1^2}, \text{ and} \\ c_1(\omega) &= \frac{b_{12}/(m_1 m_2) + j\omega/m}{j\omega}, \zeta_1 = \frac{b_{12}}{2k_{12}}\omega_1, \\ \omega_1 &= \sqrt{\frac{k_{12}m}{m_1 m_2}}, \end{aligned} \tag{4}$$

with moving mass $m = m_1 + m_2$, $m_1 = 15$ kg and $m_2 = 5$ kg, interconnected spring stiffness $k_{12} = 2.61 \times 10^7$ N/m, and damping coefficient of the single flexible mode $b_{12} = 1.98 \times 10^2$ Ns/m. The magnitude characteristics of the non-collocated plant in (4) resulting from a force being applied on mass m_1 to a position of mass m_2 are shown in Fig.2(a). The magnitude characteristics show the minus 40 dB/dec

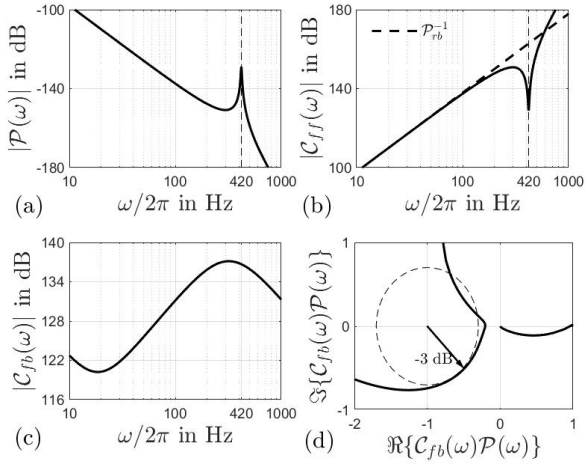

Fig. 2. Characteristics of (a) plant $\mathcal{P}(\omega)$, (b) feedforward controller $\mathcal{C}_{ff}(\omega)$, (c) feedback controller $\mathcal{C}_{fb}(\omega)$, and openloop $\mathcal{C}_{fb}(\omega)\mathcal{P}(\omega)$.

decline for the system moving as a rigid body as well as the flexible mode with resonance frequency of 420 Hz beyond which a minus 80 dB/dec decline occurs. The magnitude characteristics of the ideal feedforward controller, obtained from plant inversion, are shown in Fig.2(b). The feedback controller is given by a PID controller with a second-order low-pass filter, or

$$\mathcal{C}_{fb}(\omega) = \underbrace{k_p\left(\frac{j\omega}{\omega_d} + 1 + \frac{\omega_i}{j\omega}\right)}_{pid} \cdot \underbrace{\frac{\omega_{lp}^2}{(j\omega)^2 + 2\beta\omega_{lp}(j\omega) + \omega_{lp}^2}}_{2nd-order\ low-pass}, \tag{5}$$

with $k_p = 1.026 \times 10^6$ N/m, $\omega_d = 2\pi \times 27.5$ rad/s, $\omega_i = 2\pi \times 12.5$ rad/s, $\omega_{lp} = 2\pi \times 319.5$ rad/s, and $\beta = 0.83$. The magnitude characteristics of the feedback controller are shown in Fig.2(c), which, together with the plant in (4) lead to a controller bandwidth of 50 Hz. Robust stability of the feedback control design is shown by Nyquist evaluation in Fig.2(d), which shows anti-clockwise encirclement of the minus-one point with sufficient modulus, phase, and gain-margins, *i.e.,* sensitivity peaking of ≈ 3 dB.

Returning to the input sensitivity function in (3), sufficiently below the controller bandwidth, it generally holds that for $\omega \to 0$, $|\mathcal{C}_{fb}(\omega)\mathcal{P}(\omega)| \gg 1$, whereas $|\mathcal{P}(\omega)| \approx |\mathcal{P}_{rb}(\omega)| \gg |\mathcal{P}_{nrb}(\omega)|$; recall Example 2.1. As a result, (3) describes appropriate tracking in the sense of

$$\begin{aligned} |e(\omega)| &\leq \frac{|\mathcal{P}_{nrb}(\omega)|}{|\mathcal{P}_{rb}(\omega)|} \cdot \left|\frac{1}{1 + \mathcal{C}_{fb}(\omega)\mathcal{P}(\omega)}\right| \cdot |r(\omega)| \\ &\ll |r(\omega)| \text{ for } \omega \to 0, \end{aligned} \tag{6}$$

Contrary, if $|\mathcal{C}_{fb}(\omega)\mathcal{P}(\omega)| \ll 1$, it follows that

$$e(\omega) \approx -\sum_{i=1}^{n} \frac{c_i}{\omega^2 - 2\zeta_i\bar{\omega}_i j\omega - \bar{\omega}_i^2} \cdot \mathcal{P}_{rb}^{-1}(\omega) \cdot r(\omega), \quad (7)$$

which shows that at the natural frequencies $\bar{\omega}_i$ of the weakly-damped modes, the tracking error $e(\bar{\omega}_i) \neq 0$.

Observation 2.1: As the feedback controller $\mathcal{C}_{fb}$ plays no role in (7), a loopshaping design with notch filters chosen at the natural frequencies $\bar{\omega}_i$ does not prevent the natural frequencies $\bar{\omega}_i$ from being excited by r.

Observation 2.2: The quasi-static contribution:

$$\sum_{i=1}^{n} \frac{c_i}{\bar{\omega}_i^2}, \text{for } \omega \to 0, \quad (8)$$

can for example be taken care of by snap feedforward control, recall Example 2.1. Contrarily, the weakly-damped resonances are rarely compensated for in stage practice. This is due to the lack of robustness a higher-order feedforward controller has against machine-to-machine variation in resonance frequencies $\bar{\omega}_i$ and damping coefficients ζ_i.

Observation 2.3: As r in (7) appears affine in e, any reduction (or amplification) in frequency content of $r(\bar{\omega}_i)$ will result in an equal reduction (or amplification) of $e(\bar{\omega}_i)$. Given these observations, it makes sense to avoid exciting weakly-damped resonances by appropriate design and shaping of the reference trajectory r. This is regardless the presence (or absence) of disturbances and noises in Fig.2.

III. Fourth-order trajectories: frequency-domain analysis

For design and shaping of the reference trajectory r, let's start by considering the following definition.

Definition 3.1: For point-to-point motion, the fourth-order reference trajectory $r = r(t)$ (unit in m) is defined as

$$r(t) = \begin{cases} r_1, \text{if } t \leq \tau_1^1 \\ \underbrace{\int_{\tau_1^1}^{t} \Big\{ \int_{\tau_1^1}^{t} \Big\{ \overbrace{\int_{\tau_1^1}^{t} \Big\{ \underbrace{\int_{\tau_1^1}^{t} s(\tau)d\tau}_{=\text{ jerk } j(t) \text{ in m/s}^3} \Big\} d\tau}^{=\text{ acceleration } a(t) \text{ in m/s}^2} \Big\} d\tau \Big\} d\tau}_{=\text{ velocity } v(t) \text{ in m/s}}, \\ r_2, \text{if } t \geq \tau_2^8 \end{cases} \quad (9)$$

for $t \in (\tau_1^1, \tau_2^8)$, where snap signal $s(t)$ in m/s^4 is given by

$$s(\tau) = \begin{cases} \text{sgn}(i) \cdot s_{max}, & \text{if } \tau \in [\tau_1^i, \tau_2^i], i \in \{1, 2, \ldots, 8\}, \\ 0, & \text{elsewhere}, \end{cases} \quad (10)$$

with initial condition $v(\tau_1^1) = a(\tau_1^1) = j(\tau_1^1) = 0$ at $t = \tau_1^1$ seconds and remaining time constants (in seconds)

$$\begin{aligned} &\tau_1^i = \tau_1^{i-1} + \tau_1^2 \text{ for } i \in \{4, 6, 8\}, \tau_1^2 = \frac{a_{max}}{j_{max}}, \\ &\tau_1^3 = \frac{v_{max}}{a_{max}}, \tau_1^5 = \tau_2^4 + \tau_{scan}, \tau_1^7 = \tau_1^5 + \tau_1^3, \\ &\tau_2^i = \tau_1^i + \tau_2^1 \text{ for } i \in \{2, 3, 4, 5, 6, 7, 8\}, \tau_2^1 = \frac{j_{max}}{s_{max}}, \end{aligned} \quad (11)$$

sgn(i) represents positive/negative unity scaling:

i	1	2	3	4	5	6	7	8
sgn(i)	+1	−1	−1	+1	−1	+1	+1	−1

$\tau_{scan} = d_{scan}/v_{max}$ represents the exposure time, *i.e.,* the ratio between scanning length d_{scan} and the scanning velocity v_{max}, whereas $\tau_2^8 = 2\tau_1^5 - \tau_{scan}$ represents the end time (or period if $\tau_1^1 = 0$) of the point-to-point motion.

Example 3.1: According to Definition 3.1, consider the fourth-order reference trajectories as shown in Fig.3. For a

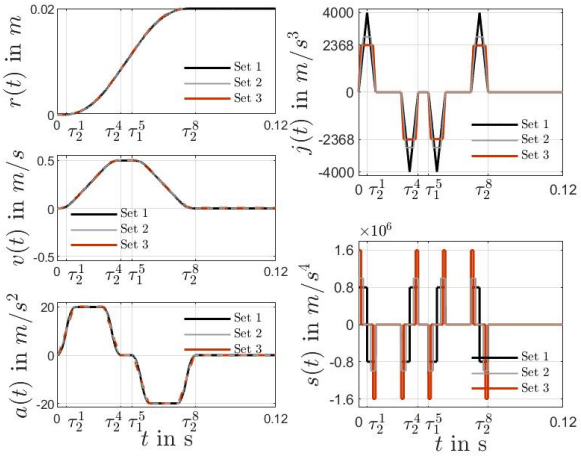

Fig. 3. Fourth-order point-to-point trajectories $r(t)$ with identical period $\tau_2^8 - \tau_1^1$ and v_{max} and a_{max}, but with different j_{max} and s_{max}.

maximum velocity of $v_{max} = 0.5$ m/s, acceleration $a_{max} = 20$ m/s^2, and three sets for jerk j_{max} and snap s_{max}:

Set1:$j_{max} = 4.0 \times 10^3$ m/s^3, $s_{max} = 8.0 \times 10^5$ m/s^4

Set2:$j_{max} = 2.7812 \times 10^3$ m/s^3, $s_{max} = 9.9686 \times 10^5$ m/s^4

Set3:$j_{max} = 2.368 \times 10^3$ m/s^3, $s_{max} = 1.6 \times 10^6$ m/s^4,

the figure shows that all trajectories are equally fast when going from the initial position $r_1 = r(\tau_1^1) = 0$ at $t = \tau_1^1 = 0$ to the final position $r_2 = r(\tau_2^8) = 0.0205$ at $t = \tau_2^8 = 0.076$. The differences are in the jerk and snap profiles. Set 1 has a triangular jerk profile with an almost two times higher value for j_{max} compared to the trapezoidal jerk profile of Set 2 and Set 3, whereas the latter has a two times higher value for s_{max}, but with the smallest duration. The time constants in (11) from Definition 3.1 associated with the three sets are given in Table I.

TABLE I
Parameter values.

Set	τ_1^1	τ_2^1	τ_1^2	τ_2^2	τ_1^3
1	0	0.0050	0.0050	0.01	0.0250
2	0	0.0028	0.0072	0.01	0.0250
3	0	0.0015	0.0085	0.01	0.0250
		τ_2^3	τ_1^4	τ_2^4	τ_{scan}
1	-	0.0300	0.0300	0.0350	0.0060
2	-	0.0278	0.0322	0.0350	0.0060
3	-	0.0265	0.0335	0.0350	0.0060

In frequency domain, s from (10) reads

$$\begin{aligned}\mathcal{F}\{s(t)\} &= \int_{-\infty}^{\infty} s(t)e^{-2\pi jft}dt \\ &= \sum_{i=1}^{8}\left\{\int_{\tau_1^i}^{\tau_2^i} \mathrm{sgn}(i)\cdot s_{max}\cdot e^{-2\pi jft}dt\right\},\end{aligned} \tag{12}$$

with $\mathcal{F}\{\cdot\}$ denoting the Fourier transform. This brings us to the first contribution and main result.

Theorem 3.1: According to Definition 3.1 trajectory $r = r(t)$ admits the following frequency-domain description:

$$\mathcal{F}\{r(t)\} = \frac{1}{2j}\cdot\frac{s_{max}}{\pi f}\cdot e^{-\pi jf\tau_2^8}\cdot\prod_{i=1}^{i=4}\frac{\sin(\pi f\tau_i)}{\pi f}, \tag{13}$$

i.e., the frequency-scaled product of four (normalized) cardinal sine functions of the form $\sin(\pi x)/\pi x$.

Proof: For $i = 1$ in (12), Fourier analysis gives

$$\begin{aligned}&\int_0^{\tau_2^1} s_{max}\cdot e^{-2\pi jft}dt = -\frac{s_{max}}{2\pi jf}\cdot e^{-2\pi jft}\Big|_0^{\tau_2^1} \\ &= 2j\cdot\frac{s_{max}}{2\pi jf}\cdot e^{-\pi jf\tau_2^1}\cdot\frac{1}{2j}\cdot\left(e^{\pi jf\tau_2^1} - e^{-\pi jf\tau_2^1}\right) \\ &= \frac{s_{max}}{\pi f}\cdot e^{-\pi jf\tau_2^1}\cdot\sin(\pi f\tau_2^1).\end{aligned} \tag{14}$$

Similar for $i = 2$, which, when compared to (14), features a time-shift τ_1^2 as well as a sign change, it follows that

$$\begin{aligned}&-\int_{\tau_1^2}^{\tau_1^2+\tau_2^1} s_{max}\cdot e^{-2\pi jft}dt \\ &= -e^{-2\pi jf\tau_1^2}\cdot\int_0^{\tau_2^1} s_{max}\cdot e^{-2\pi jft}dt \\ &= -\frac{s_{max}}{\pi f}\cdot e^{-2\pi jf\tau_1^2}\cdot e^{-\pi jf\tau_2^1}\cdot\sin(\pi f\tau_2^1).\end{aligned} \tag{15}$$

Adding up both contributions gives

$$\begin{aligned}&\sum_{i=1}^{2}\left\{\int_{\tau_1^i}^{\tau_2^i}\mathrm{sgn}(i)\cdot s_{max}\cdot e^{-2\pi jft}dt\right\} \\ &= (1-e^{-2\pi jf\tau_1^2})\cdot\int_0^{\tau_2^1} s_{max}\cdot e^{-2\pi jft}dt \\ &= 2j\cdot e^{-\pi jf\tau_1^2}\cdot\frac{1}{2j}\cdot\left(e^{\pi jf\tau_1^2} - e^{-\pi jf\tau_1^2}\right)\cdot\ldots \\ &\qquad\qquad\ldots\int_0^{\tau_2^1} s_{max}\cdot e^{-2\pi jft}dt \\ &= 2j\cdot\frac{s_{max}}{\pi f}\cdot e^{-\pi jf(\tau_2^1+\tau_1^2)}\cdot\sin(\pi f\tau_1^2)\cdot\sin(\pi f\tau_2^1).\end{aligned} \tag{16}$$

Repeating the argument for the combined contributions of $i = 3$ and $i = 4$, that is, using (16) and applying a time shift of τ_1^3 as well as a sign change, it follows that

$$\begin{aligned}&\sum_{i=3}^{4}\left\{\int_{\tau_1^i}^{\tau_2^i}\mathrm{sgn}(i)\cdot s_{max}\cdot e^{-2\pi jft}dt\right\} \\ &= -e^{-2\pi jf\tau_1^3}\cdot\sum_{i=1}^{2}\left\{\int_{\tau_1^i}^{\tau_2^i}\mathrm{sgn}(i)\cdot s_{max}\cdot e^{-2\pi jft}dt\right\}.\end{aligned} \tag{17}$$

Combining (17) with (16) gives for the complete acceleration phase $t\in[\tau_1^1,\tau_2^4]$,

$$\begin{aligned}&\sum_{i=1}^{4}\left\{\int_{\tau_1^i}^{\tau_2^i}\mathrm{sgn}(i)\cdot s_{max}\cdot e^{-2\pi jft}dt\right\} \\ &= (1-e^{-2\pi jf\tau_1^3})\cdot\sum_{i=1}^{2}\left\{\int_{\tau_1^i}^{\tau_2^i}\mathrm{sgn}(i)\cdot s_{max}\cdot e^{-2\pi jft}dt\right\} \\ &= 2j\cdot e^{-\pi jf\tau_1^3}\cdot\frac{1}{2j}\cdot\left(e^{\pi jf\tau_1^3} - e^{-\pi jf\tau_1^3}\right)\cdot\ldots \\ &\qquad\ldots\sum_{i=1}^{2}\left\{\int_{\tau_1^i}^{\tau_2^i}\mathrm{sgn}(i)\cdot s_{max}\cdot e^{-2\pi jft}dt\right\} \\ &= (2j)^2\cdot\frac{s_{max}}{\pi f}\cdot e^{-\pi jf(\tau_2^1+\tau_1^2+\tau_1^3)}\cdot\sin(\pi f\tau_1^3)\cdot\ldots \\ &\qquad\ldots\sin(\pi f\tau_1^2)\cdot\sin(\pi f\tau_2^1).\end{aligned} \tag{18}$$

Similarly for the deceleration phase $t\in[\tau_1^5,\tau_2^8]$, so after time shift $\tau_1^5 = \tau_2^1+\tau_1^2+\tau_1^3+\tau_{scan}$ and opposite signs, it holds that

$$\begin{aligned}&\sum_{i=5}^{8}\left\{\int_{\tau_1^i}^{\tau_2^i}\mathrm{sgn}(i)\cdot s_{max}\cdot e^{-2\pi jft}dt\right\} \\ &= -e^{-2\pi jf\tau_1^5}\cdot\sum_{i=1}^{4}\left\{\int_{\tau_1^i}^{\tau_2^i}\mathrm{sgn}(i)\cdot s_{max}\cdot e^{-2\pi jft}dt\right\},\end{aligned} \tag{19}$$

which for the last term in (12) and by using $\tau_2^8 = 2\tau_1^5 - \tau_{scan}$ leads to

$$\begin{aligned}\mathcal{F}\{s(t)\} &= \sum_{i=1}^{8}\left\{\int_{\tau_1^i}^{\tau_2^i}\mathrm{sgn}(i)\cdot s_{max}\cdot e^{-2\pi jft}dt\right\} \\ &= \left(1-e^{-2\pi jf\tau_1^5}\right)\cdot\sum_{i=1}^{4}\left\{\int_{\tau_1^i}^{\tau_2^i}\mathrm{sgn}(i)\cdot s_{max}\cdot e^{-2\pi jft}dt\right\} \\ &= 2j\cdot e^{-\pi jf\tau_1^5}\cdot\frac{1}{2j}\cdot\left(e^{\pi jf\tau_1^5} - e^{-\pi jf\tau_1^5}\right)\cdot\ldots \\ &\qquad\ldots\sum_{i=1}^{4}\left\{\int_{\tau_1^i}^{\tau_2^i}\mathrm{sgn}(i)\cdot s_{max}\cdot e^{-2\pi jft}dt\right\} \\ &= (2j)^3\cdot\frac{s_{max}}{\pi f}\cdot e^{-\pi jf\tau_2^8}\cdot\sin(\pi f\tau_2^8)\cdot\sin(\pi f\tau_1^3)\cdot\ldots \\ &\qquad\ldots\sin(\pi f\tau_1^2)\cdot\sin(\pi f\tau_2^1).\end{aligned} \tag{20}$$

Four times integration of $\mathcal{F}\{s(t)\}$ gives in frequency domain

$$\mathcal{F}\{r(t)\} = \frac{\mathcal{F}\{s(t)\}}{(2\pi jf)^4}, \tag{21}$$

which together with (20) yields (13). ∎

Observation 3.1: From (13), it is clear that $\mathcal{F}\{r(t)\}$ has no spectral content at frequencies $f\in\{1/\tau_2^8, 1/\tau_1^3, 1/\tau_1^2, 1/\tau_2^1\}$, or natural multiples thereof.

Observation 3.2: For $f\to 0$, (13) shows a 20 dB/dec decline in frequency content, which is identical to the attenuation obtained for a point-to-point motion with either a second- or third-order trajectory. For $f\to\infty$, a 100 dB/dec

attenuation results, which gives 20 dB/dec more attenuation with respect to a third-order trajectory, and 40 dB/dec more attenuation than with a second-order trajectory.

Observation 3.3: For fixed $a_{max}, v_{max}, \tau_{scan}$, it follows from Definition 3.1 that a point-to-point motion with a fourth-order trajectory takes $2\tau_2^1$ seconds longer than a similar motion with a third-order trajectory, and $2\tau_2^2 = 2\tau_2^1 + 2\tau_1^2$ seconds longer than again a similar motion but with a second-order trajectory. This shows a penalty on time needed to conduct point-to-point motions for increased order.

IV. Application to Wafer Scanners

For wafer scanners, increasing the order of the reference trajectories may come with decreased wafer throughput, but not necessarily at the expense of wafer yield, *i.e.,* the amount of effective chips being processed per time unit — nowadays wafer scanners either use fourth- or third-order trajectories. While throughput may drop from increasing order, the accuracy of servo positioning generally improves. This leads to reduced losses in terms of defective chips, and as such a positive effect on wafer yield. The next result shows how to influence yield in a throughput-invariant manner.

Corollary 4.1: Let τ_2^8, τ_{scan}, a_{max}, and v_{max} be fixed (specified) values. The frequencies $1/\tau_1^2, 1/\tau_2^1$ (or natural multiples thereof) at which r from Definition 3.1 has no spectral content can be chosen freely for all pairs (τ_1^2, τ_2^1) under the following conditions:

(a) $\tau_1^2 + \tau_2^1 = c_1$,
(b) $\frac{1}{2}c_1 \leq \tau_1^2 \leq c_2$,
(c) $c_3 \leq \tau_2^1 \leq c_4$,

with time constants $c_1 = \tau_2^2$, $c_2 = c_1 - j_{max}^{lower}/s_{max}^{upper}$, $c_3 = j_{max}^{lower}/s_{max}^{upper}$, $c_4 = j_{max}^{upper}/s_{max}^{lower}$, and $j_{max} \in [j_{max}^{lower}, j_{max}^{upper}]$, $s_{max} \in [s_{max}^{lower}, s_{max}^{upper}]$.

Proof: The proof is graphically shown in Fig.4, but

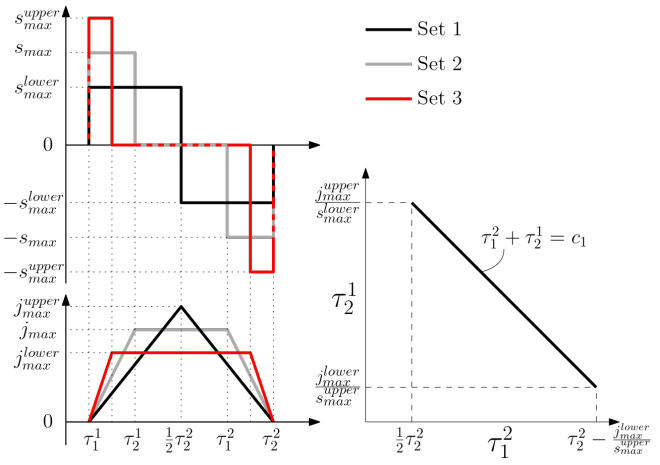

Fig. 4. Snap-jerk free parameter space of fourth-order trajectory r.

also follows from

$$\begin{aligned}\tau_2^8 &= 2\tau_1^5 - \tau_{scan} \text{ (or with } \tau_1^5 = \tau_2^4 + \tau_{scan}) \\ &= 2\tau_2^4 + \tau_{scan} \text{ (or with } \tau_2^4 = \tau_1^4 + \tau_2^1 = \tau_1^3 + \tau_1^2 + \tau_2^1) \\ &= 2\tau_1^3 + 2\tau_1^2 + 2\tau_2^1 + \tau_{scan}. \end{aligned} \tag{22}$$

With τ_2^8, τ_{scan}, a_{max}, v_{max} being fixed values and τ_1^3 constant, $\tau_1^2 + \tau_2^1 = \tau_2^2$ in (22) must be constant too. The ranges $j_{max}^{lower} \leq j_{max} \leq j_{max}^{upper}$, $s_{max}^{lower} \leq s_{max} \leq s_{max}^{upper}$ shown in Fig.4 allow for freely choosing pairs (τ_1^2, τ_2^1) that satisfy $\tau_1^2 + \tau_2^1 = \tau_2^2$ and by design keep τ_2^8, τ_{scan}, a_{max}, and v_{max} at specified values, which completes the proof. ■

Example 4.1: In line with Theorem 3.1, the motivation for the three sets in Fig.3 of Section III stems from frequency-domain evaluation as shown in Fig.5. Here, it can be seen

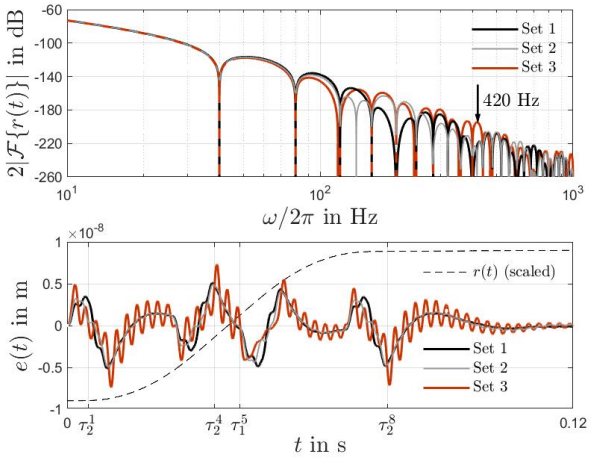

Fig. 5. Magnitude spectra of $\mathcal{F}\{r(t)\}$ for three fourth-order point-to-point motions $r(t)$ that have identical duration τ_2^8, and motion parameters v_{max}, and a_{max}, but different j_{max} and s_{max}.

that Set 1 and Set 2 (as opposed to Set 3) are designed to have significantly less spectral content around the weakly-damped resonance frequency of 420 Hz, recall Example 2.1. The result will be less excitation of the associated structural mode under closed-loop control. This is shown in the bottom part of the figure by time-series responses.

From Example 4.1, it becomes clear that (high-frequency) tracking accuracy during exposure can be improved in a throughput-invariant manner by appropriate pairing of j_{max} and s_{max}. This brings us to the second contribution.

Proposition 4.1: Consider r from Definition 3.1 which satisfies the conditions from Corollary 4.1. The pair (τ_1^2, τ_2^1) that minimizes the closed-loop error signal $e(t)$ for the time interval $t \in [\tau_1^1, \tau_2^8]$ in an $\mathcal{L}_\infty$ sense is given by

$$\begin{aligned} \underset{(\tau_1^2, \tau_2^1)}{\text{minimize}} \quad & \|e(t)\|_\infty \\ \text{subject to} \quad & \tau_1^2 + \tau_2^1 = c_1 \\ & \frac{1}{2}c_1 \leq \tau_1^2 \leq c_2 \\ & c_3 \leq \tau_2^1 \leq c_4. \end{aligned} \tag{23}$$

Proposition 4.1 represents a semi-definite program that typically can be solved using interior point methods. In view of Corollary 4.1 and Proposition 4.1, Fig.6 shows the optimal Set 2 for the pair (j_{max}, s_{max}) around $j_{max} = 2823$ m/s^3 and $s_{max} = 9.7 \times 10^5$ m/s^4. Set 2 induces an error of

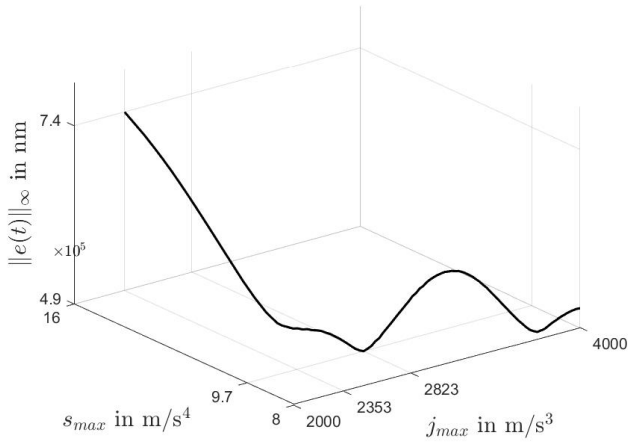

Fig. 6. $\|e(t)\|_\infty$ for $t \in [\tau_1^1, \tau_2^8]$ and various pairs (τ_1^2, τ_2^1) from fourth-order point-to-point motions $r(t)$ that have identical $r(t)$, $v(t)$, $a(t)$ but different pairs $(j(t), s(t))$.

$\|e(t)\|_\infty = 4.86$ nm, which is slightly better than the performance obtained with Set 1 of $\|e(t)\|_\infty = 5.14$ nm, but significantly better than the performance obtained with Set 3 of $\|e(t)\|_\infty = 7.4$ nm.

Remark 4.1: Different from the unfiltered $\mathcal{L}_\infty$ context in Proposition 4.1, one could argue that the use of filtered signals like moving average or moving standard deviation error signals as used in wafer scanner applications could be useful. As the moving average filter operation in frequency domain can be represented by a (normalized) cardinal sine function, this does come at the risk of becoming insensitive to specific resonance frequencies that could be relevant to stage positioning. Alternatively, $\mathcal{L}_2$ or $\mathcal{L}_{rms}$ can be considered. However, as these reflect the summation of energy contributions over all frequencies, they appear less sensitive to (and suited for) shaping of reference trajectories dedicated to individual frequency contributions.

Remark 4.2: Scanning multiple fields on a wafer is done by constructing a sequence of point-to-point motions. In the trajectory generation, the maximum values as well as the ratios jerk-over-acceleration and snap-over-jerk are kept constant, *i.e.,* all generated trajectories essentially have identical frequency-domain characteristics. As such, the computation time needed to solve the semi-definite program in Proposition 4.1 does not play a role during wafer scanner operation.

V. Conclusions

Appropriately pairing snap and jerk values in fourth-order reference trajectories is shown to be effective when dealing with motion systems with weakly-damped modes. This pairing offers improvements to stage reference tracking that need not come at the expense of throughput, and may contribute to the improvement of wafer yield instead.

References

[1] Heertjes MF., Butler H., Dirkx NJ., van der Meulen SH., Ahlawat R., O'Brien K., Simonelli J., Teng K-T., and Zhao Y. Control of wafer scanners: methods and developments, American Control Conference, Denver, CO, pp. 3686-3703, 2020.

[2] Butler, H. Position control in lithographic equipment. IEEE Control Systems Magazine, 31(5) pp. 28-47, 2011.

[3] Boerlage M.L.G., Tousain R.L., Steinbuch M., Jerk derivative feedforward control for motion systems. In Proc. of the American Control Conference, Boston, MA, pp. 4843-4848, 2004.

[4] Van der Meulen SH., Tousain RL., and Bosgra OH., Fixed structure feedforward controller design exploiting iterative trials: application to a wafer stage and a desktop printer. J. of Dynamic Systems, Measurement, and Control, 130(5), pp. 051006 (16 pages), https://doi.org/10.1115/1.2957626.

[5] Boeren FAJ., Bruijnen DJH., and Oomen TAE. Enhancing feedforward controller tuning via instrumental variables: with application to nanopositioning. Int. J. of Control, 90(4), pp. 746-764, 2017.

[6] Kontaras N., Heertjes M.F., and Zwart H., Continuous compliance compensation of position-dependent flexible structures. IFAC PapersOnline, 49(13), pp. 76-81, 2016.

[7] Smith OJM. Posicast control of damped oscillatory systems, Proc. of the IRE, pp. 1249-1255, 1957.

[8] Smith, OJM. Feedback Control Systems, McGraw-Hill series in control systems engineering, New York, USA, 1958.

[9] Singer NC., and Seering WP., Preshaping command inputs to reduce system vibration. J. of Dynamic Systems, Measurement, and Control, 112(77), pp.76-82, 1990.

[10] Singhose WE., Seering WP., and Singer N.C., Input shaping for vibration reduction with specified insensitivity to modeling errors, Proc. of the 1996 Japan-U.S.A. Symposium on Flexible Automation, ASME, Boston, MA, 1996.

[11] Pao, LY., Multi-input shaping design for vibration reduction. Automatica, 35(1), pp. 81-89, 1999.

[12] Singhose W., Command shaping for flexible systems: a review of the first 50 years. Int. J. of Precision Engineering and Manufacturing, 10(4), pp.153-168, 2009.

[13] Kang C-G., Hassan R., and Kim K-Y., Analysis of a generalized ZVD shaper using impulse vectors. Int. J. of Control, Automation and Systems, 18(8), pp. 2088-2094, 2020.

[14] Bhat S.P., and Miu D.K., Precise Point-to-Point Positioning Control of Flexible Structures, J. of Dynamic Systems, Measurement, and Control, 112, pp. 667-674, 1990.

[15] Béarée R., New Damped-Jerk trajectory for vibration reduction. Control Engineering Practice, 28, pp. 112-120, 2014.

[16] Al-Rawashdeh YM., Al Janaideh M., and Heertjes, MF., On step-and-scan trajectories used in wafer scanners in semiconductor manufacturing. IEEE/RSJ Int. Conf. on Intelligent Robots and Systems (IROS), Prague, Czech Republic, pp. 7580-7586, 2021.

[17] Sencer B., and Tajima S., Frequency optimal feed motion planning in computer numerical controlled machine tools for vibration avoidance. J. of Manufacturing Science and Engineering, 139, pp. 011006, 2017.

[18] Sencer B., Dumanli A., and Yamada Y., Spline interpolation with optimal frequency spectrum for vibration avoidance. CIRP Annals, 67(1), pp. 377-380, 2018.

[19] Dumanli A., Sencer B., Robust trajectory generation for multiaxis vibration avoidance. IEEE/ASME Trans. on Mechatronics, 25(6), pp.2938-2949, 2020.

[20] Biggelaar Van den P.M.C.M., Cox H.H.M., Tso Y.T., Donders S.N.L., and Knoop T., Lithographic apparatus and device manufacturing method, ASML Netherlands B.V., United States Patent, US 7,016,019 B2, 2006.

[21] Lambrechts P., Boerlage M., and Steinbuch M. Trajectory planning and feedforward design for electromechanical motion systems, Control Engineering Practice, 13, pp. 145-157, 2005.

[22] Singh T., and Vadali S.R., Robust time-optimal control: frequency doamin approach. J. of Guidance, Control, and Dynamics, 17(2), pp. 346-353, 1994.

[23] Bai Y., Chen X., Sun H., and Yang Z., Time-optimal freeform s-curve profile under positioning error and robustness constraints. IEEE/ASME Trans. on Mechatronics, 23(4), pp. 1993-2003, 2018.

[24] Miu D.K., Bhat S.P., Solutions of Point to point Control Problems Using Laplace Transform Technique, ASME J. of Dynamic Systems,Measurement, and Control, Vol. 113, pp. 425-431 , 1991.

[25] Al-Masoud N., Chu S-Y, and Singh T., Discrete-time point-to-point control of flexible structures. In Proc. of American Control Conference, Chicago, Ilinois, pp. 2433-2437, 2000.